



Published in final edited form as:

*Math Biosci.* 2016 August ; 278: 11–21. doi:10.1016/j.mbs.2016.05.001.

## The role of electrical coupling in generating and modulating oscillations in a neuronal network

Christina Mouser<sup>\*</sup>, Amitabha Bose<sup>†</sup>, and Farzan Nadim<sup>‡</sup>

Christina Mouser: mouser@c@wpunj.edu; Amitabha Bose: bose@njit.edu; Farzan Nadim: farzan@njit.edu

<sup>\*</sup>Department of Mathematics, William Paterson University, Wayne, NJ 07470

<sup>†</sup>Department of Mathematical Sciences, New Jersey Institute of Technology, Newark, NJ 07102

<sup>‡</sup>Federated Department of Biological Sciences, New Jersey Institute of Technology and Rutgers University, Newark, NJ 07102

### Abstract

A simplified model of the crustacean gastric mill network is considered. Rhythmic activity in this network has largely been attributed to half center oscillations driven by mutual inhibition. We use mathematical modeling and dynamical systems theory to show that rhythmic oscillations in this network may also depend on, or even arise from, a voltage-dependent electrical coupling between one of the cells in the half-center network and a projection neuron that lies outside of the network. This finding uncovers a potentially new mechanism for the generation of oscillations in neuronal networks.

### Keywords

electrical coupling; half-center oscillator; phase-plane analysis

## 1 Introduction

Networks of neurons display a variety of oscillatory behaviors. For example, oscillations in the levels of calcium concentrations, gene expressions and in the membrane voltage across cell membranes are all commonly found in neuronal systems. Often these oscillations are rhythmic in that they display a consistent pattern at a prescribed frequency [1]. Central pattern generating (CPG) networks provide several examples that exhibit rhythmic activity. CPGs refer to networks of neurons in the central nervous system that produce patterned (usually oscillatory) activity in the absence of patterned sensory input. These networks play a critical role in generating a diverse array of motor functions such as digestion, locomotion, respiration and regulation of heartbeat in invertebrates [2]. A central question in the study of

### Conflict of Interest

The authors declare that they have no conflict of interest.

**Publisher's Disclaimer:** This is a PDF file of an unedited manuscript that has been accepted for publication. As a service to our customers we are providing this early version of the manuscript. The manuscript will undergo copyediting, typesetting, and review of the resulting proof before it is published in its final citable form. Please note that during the production process errors may be discovered which could affect the content, and all legal disclaimers that apply to the journal pertain.

neural oscillations is what are the mechanisms that underlie the generation of rhythmic activity and how that activity is regulated. This study will focus on this general question in the context of the gastric mill rhythm (GMR; frequency 0.1 Hz) that arises in the stomatogastric ganglion (STG) in the crustacean central nervous system. In particular, we will show the existence of a new mechanism based on voltage-dependent electrical coupling for generation of oscillations within a neuronal network.

The gastric mill network consists of a small number of neurons in the STG that control muscles that move teeth to provide grinding of food (chewing) within the gastric mill stomach of crustaceans [3]. In the Jonah crab, a pair of neurons, the lateral gastric (*LG*) and Interneuron 1 (*INT1*) form a half-center oscillator (HCO) and are primary contributors to the GMR. These neurons are connected by reciprocally inhibitory synapses and, during gastric mill activity, display anti-phase bursting oscillations. They also receive input from various parts of the stomatogastric nervous system (STNS). In particular, *INT1* receives rhythmic inhibition from the pacemaker anterior burster neuron (*AB*) of the pyloric CPG. Because the pyloric rhythm (frequency 1 Hz) is much faster than the gastric mill, the *AB* to *INT1* input produces pyloric timed patterns in the *INT1* bursting activity. Both *LG* and *INT1* receive excitatory input from the modulatory commissural neuron 1 (*MCM1*) with *INT1* receiving fast excitation and *LG* receiving slow modulatory excitation. Additionally, the *MCM1* axon terminals are electrically coupled to *LG* in a manner that is dependent on the voltage of *LG* [5]. It is the role of this electrical coupling that is of particular interest to us in this paper.

Neurons that lie within a HCO typically utilize reciprocal inhibition to generate oscillations [6]. In particular, in a two cell HCO, when one of the cells is active, its inhibitory synapse suppresses the other. At some later time, the silent cell escapes or is released from inhibition and the roles of the two cells switch [7]. In the gastric mill network, *LG* and *INT1* can oscillate in this manner with the ability to escape inhibition and generate oscillations, but only in the presence of the excitatory input provided by *MCM1* [5, 8].

Although a number of modeling studies have explored the generation of oscillations in the gastric mill network [8, 9, 10, 11, 13], the role of the strong electrical coupling between the *MCM1* axon terminals and the *LG* neuron has not been previously explored. In this study, we will show that voltage-dependent electrical coupling can provide an alternative mechanism for the generation of oscillations when the inhibition based HCO mechanism is incapable of doing so. In particular the *LG* – *INT1* HCO can be rendered ineffective if 1) the inhibitory synapse from *INT1* to *LG* is inactivated, or 2) if the excitability property of *LG* is reduced. In order to fully understand how electrical coupling affects this network, we will first consider a simple model to see how electrical coupling between *LG* and *MCM1* axon terminals affects the ability of oscillations to be created through the standard HCO inhibition based mechanism. We will discuss how the electrical coupling modulates the rhythmic properties of this oscillation. We will then remove the *INT1* to *LG* synapse and show that rhythmic oscillations can still arise through the electrical coupling between *LG* and *MCM1* axon terminals, but only if this coupling is voltage dependent, as has been reported experimentally [5]. We will then demonstrate the same in a biophysical model based on the Morris-Lecar equations [15]. For both models, we derive conditions on parameters showing why the electrical coupling must be voltage dependent to produce oscillations.

The modeling and analysis in this paper is based on the use of geometric singular perturbation theory. Exploiting inherent differences in timescales, we will derive sets of fast and slow equations that can be studied in the relevant phase space. For the simple model, this can be done on a two-dimensional phase plane and is the focus of Sections 3.1–3.4. The analysis in those sections follows the tradition of using relaxation oscillators with the individual neurons modeled as passive elements. The relaxation oscillations in this case arise due to the method of model reduction that incorporates a slow synaptic variable. In Section 3.5, the fast-slow analysis allows us to project the relevant dynamics onto two different phase planes to facilitate understanding of the model.

## 2 Model

### 2.1 Simple passive cell network model

We describe the simple network that we shall initially consider. A key assumption for this model is that *INT1* and *LG* are modeled as passive cells with no active currents or excitable properties. Thus if oscillations are to be generated, they must arise as a direct result of network interactions. By identifying variables that evolve on different time scales and by making a few other assumptions, we can use geometric singular perturbation theory to focus on the analysis of a reduced two-dimensional system of equations. These variables correspond to the voltage of *LG* and to the synaptic input that *LG* receives from *MCN1* and are shown in solid in Fig. 1. The electrical coupling is also shown in solid in Fig. 1 as it can be defined in terms of the reduced quantities including the voltage of *LG*. Shown with dotted lines/circles are the other variables that we will incorporate into the solid variables and thus will not need to explicitly track.

Let  $V_L$  and  $V_I$  denote the voltages of *LG* and *INT1* respectively. We will not model individual spikes but instead keep track of when a cell is above (active) or below (silent) threshold. These voltages will evolve on a fast time scale. Notice that *AB* and *MCN1* do not receive synaptic input from any other cells in the circuit. Thus we do not explicitly model either but instead need only keep track of their synaptic and electrical output. The equations that describe the relevant voltages are:

$$\varepsilon \frac{dV_L}{dt} = -I_{rest,L}(V_L) - I_{syn,I \rightarrow L}(V_I, V_L) - I_{syn,M \rightarrow L}(V_M, V_L, s) - I_{elec}(V_L, V_M) \quad (1)$$

$$\varepsilon \frac{dV_I}{dt} = -I_{rest,I}(V_I) - I_{syn,L \rightarrow I}(V_I, V_L) - I_{syn,AB \rightarrow I}(V_I, s_{AB \rightarrow I}) \quad (2)$$

The intrinsic current  $I_{rest,x}(V_x) = g_{rest,x}[V - E_{rest,x}]$  where  $g_{rest,x}$  and  $E_{rest,x}$  are the passive rest conductance and reversal potentials. Notice that in the absence of any other currents, the value  $V = E_{rest,x}$  is a stable rest point. For *LG*,  $E_{rest,L} < V_T$  while for *INT1*,  $E_{rest,I} > V_T$  for a fixed threshold  $V_T$ . *MCN1* is assumed to be tonically active which we model by setting its voltage to a value  $V_M > V_T$ . The synaptic currents obey an equation of the form  $I_{syn,x \rightarrow y} = g_{x \rightarrow y} s_{x \rightarrow y} [V_y - E_{inh}]$  where  $x$  and  $y$  are the pre- and post-synaptic cells. The variables

$s_{AB \rightarrow I}$ ,  $s_{L \rightarrow I}$  and  $s_{I \rightarrow L}$  are straight forward to understand and are instantaneous. The synaptic variable  $s_{AB \rightarrow I}$  provides the input due to  $AB$  activity and is modeled using a periodic, half-sine function with an amplitude of 1 and period of 1 second. This synapse takes on the value one when the sine function is greater than a threshold, set here to 0.5, and is zero otherwise. The synapses between  $LG$  and  $INT1$  are also instantaneous and we utilize the fact that these cells are always out-of-phase with one another.

$$s_{AB \rightarrow I}(t) = \text{Heav}\left(\sin\left(\frac{2\pi(t)}{1000}\right) - 0.5\right) \quad (3)$$

$$s_{L \rightarrow I}(V_L) = \left[1 + \exp\left(\frac{v_1 - V_L}{k_1}\right)\right]^{-1} \quad (4)$$

$$s_{I \rightarrow L}(V_I) = \left[1 + \exp\left(\frac{v_2 - V_I}{k_2}\right)\right]^{-1} \quad (5)$$

The remaining synaptic variable  $s$  requires some explanation. In the biological system,  $MCM1$  exerts a slow excitatory effect on  $LG$  that is modulated by pre-synaptic inhibition from  $LG$  onto the  $MCM1$  to  $LG$  synapse. Thus when  $LG$  is active, this excitation is slowly removed; when  $LG$  is silent, the excitation slowly builds. This is modeled by the variable  $s$  that evolves on a slow time scale and is the only slow variable in our model. Equations governing this variable are:

$$\frac{ds}{dt} = \begin{cases} (1-s)/\tau_r & V_L \leq V_T \\ -s/\tau_f & V_L > V_T \end{cases} \quad (6)$$

In equation (1), the synaptic current is then given by

$$I_{syn, M \rightarrow L} = g_{M \rightarrow L} s [V_L - E_{exc}]. \quad (7)$$

Figure 1 shows an electrical coupling between  $LG$  and the  $MCM1$  axon terminals. The electrical current is given by

$$I_{elec}(V_L, V_M) = g_{elec}(V_L) [V_L - V_M]. \quad (8)$$

This coupling is dependent on the voltage of  $LG$  and  $MCM1$  in two different ways. First, the strength is an increasing function of  $V_L$ . The dependency of the conductance  $g_{elec}$  on  $V_L$  is

incorporated using an increasing sigmoidal function  $n_\infty(V_L)$ . Second this strength is dependent on the driving force which is the difference between the  $LG$  and  $MCM1$  voltages. In the biological system, the electrical coupling has a minimal effect on the MCN1 voltage[5], almost as if the electrical coupling were rectifying. We model this by simply keeping the  $MCM1$  voltage fixed at  $V_M$  independent of the value of  $V_L$ . We define

$$g_{elec}(V_L) = \bar{g}_{elec} n_\infty(V_L) \quad (9)$$

where

$$n_\infty(V_L) = (1 - g_{min}) \left( 1 + \exp\left(\frac{v_{el} - V_L}{k_{el}}\right) \right)^{-1} + g_{min}. \quad (10)$$

where  $v_{el}$  is the half activation value at which  $n_\infty(V_L) = (1 - g_{min})/2$  and  $k_{el}$  is the reciprocal of the slope at that point. The asymptotic value of  $n_\infty(V_L)$  as  $V_L \rightarrow -\infty$  is denoted by  $g_{min} \in (0, 1)$  and is the smallest positive value of the electrical conductance.

While, equations (1)–(8) govern the flow of the gastric mill circuit, the dynamics can be simplified by exploiting the small parameter  $\varepsilon$  that demarcates the fast and slow time scales, as was first done by Kintos et. al. [11]. Set  $\varepsilon = 0$  in (1)–(2). The latter of these equations can be rewritten in terms of  $V_L$  and of the independently controlled quantity  $s_{AB \rightarrow I}$ . Namely, from (2), note that we can solve for  $V_I = h_1(V_L, s_{AB \rightarrow I})$ ; see the Appendix. Thus the set of equations governing the slow flow can be reduced to

$$0 = -g_{rest,L} [V_L - E_{rest,L}] - g_{I \rightarrow L} s_{I \rightarrow L} (h_1(V_L, s_{AB \rightarrow I})) [V_L - E_{inh}] - g_{M \rightarrow L} s [V_L - E_{exc}] - g_{elec}(V_L, V_M) [V_L - V_M] \quad (11)$$

$$\frac{ds}{dt} = \begin{cases} (1-s)/\tau_r & V_L \leq V_T \\ -s/\tau_f & V_L > V_T. \end{cases} \quad (12)$$

Denote the right-hand side of (11) by  $F(V_L, s)$ . The first equation constrains the flow to lie on  $F(V_L, s) = 0$ , and slaves the evolution of  $V_L$  to  $s$  which is governed by the second equation (12). Rescale  $t = \varepsilon \tau$ , then set  $\varepsilon = 0$  to obtain the fast equations

$$\frac{dV_L}{d\tau} = F(V_L, s) \quad (13)$$

$$\frac{ds}{d\tau} = 0. \quad (14)$$

Equations (13–14) govern the fast jumps that a trajectory in the phase plane makes between different possible (stable) branches of the  $V_L$ -nullcline. For  $\varepsilon$  small enough, an actual solution to (1)–(8) lies  $\mathcal{O}(\varepsilon)$  close to a singular periodic orbit which is pieced together from solutions of (11)–(14).

The  $V_L$  nullcline is the set of points  $\{(V_L, s) : F(V_L, s) = 0\}$  and can be graphed by explicitly solving for  $s$  to obtain

$$s = \frac{-g_{rest,L}[V_L - E_{rest,L}] - g_{I \rightarrow L} s_{I \rightarrow L} (h_1(V_L, s_{AB \rightarrow I})) [V_L - E_{inh}] - g_{elec}(V_L)[V_L - V_M]}{g_{M \rightarrow L}[V_L - E_{exc}]} \quad (15)$$

The  $s$ -nullcline is simply the Heaviside function given by  $s = 1$  when  $V_L < V_T$  and  $s = 0$  when  $V_L > V_T$ . We could smooth this nullcline out to a sigmoid with no qualitative change in results.

The shape of the  $V_L$ -nullcline is dependent on our choice of parameters. It is known from prior modeling work of this system [11, 12], and of many others in different contexts, that when one of the nullclines is cubic shaped and the other is linear or sigmoidal that oscillations may occur if the nullclines intersect on the middle branch of the cubic. In the results section below we will show how various parameters related to both the synaptic and electrical coupling affect the shape of the  $V_L$  nullcline and allow it to be a cubic.

## 2.2 Biophysical model

In Section 3.5, we will use the Morris-Lecar equations to model both  $LG$  and  $INT1$ . As a result of the added dimensionality of the model, we will not be able to reduce the analysis to a two-dimensional phase plane. However, similar to our analysis with the simple model, we will be able to show that the projection of the  $LG$  trajectory onto two distinct two-dimensional phase planes will be crucial to understanding the role of voltage-dependent electrical coupling. When parameters are chosen in the Morris-Lecar equations to reduce the excitability of  $LG$ , the inhibition based HCO becomes ineffective. In that case, as in the case of the simple model, electrical coupling will be able to produce oscillations but only when it is voltage-dependent. Details of the model will be provided in Section 3.5 and the Appendix.

## 3 Results

### 3.1 Oscillations that arise through the $INT1$ - $LG$ reciprocal inhibition

For completeness and for ease in explaining the role of the voltage dependent electrical coupling, we begin by reviewing the case when  $\tilde{g}_{elec} = 0$  as described in [10]. Oscillations in this case arise as a direct consequence of the mutually inhibitory pair  $INT1$  and  $LG$ . Because of different synaptic strengths between the two and different time constants in the active and

silent states of  $LG$ , the cells form an asymmetric half-center oscillator (HCO) in that the duty cycle of each cell is not equal to  $1/2$ . They do, however, oscillate in anti-phase where only one of the cells is active at any moment in time.

First set  $g_{AB \rightarrow I} = 0$  meaning that  $AB$  inhibition to  $INT1$  is absent. We choose similar parameter values to [10] such that the  $V_L$ -nullcline is then a cubic shaped curve where the left and right branches are positively sloped; see the left panel of Fig. 2A. Except for the local extrema, points that lie on the left and right branches are stable fixed points of the fast equations (13). The threshold  $V_T$  is chosen to intersect the middle branch of the cubic nullcline. The solution trajectory for this case is easy to understand. Starting at the local maximum of the left branch, equation (13) is used to make a fast jump to the right branch. Note that this jump is horizontal since  $ds/d\tau = 0$  according to (14). Then (11)–(12) are used to evolve the slow flow down the right branch until the trajectory reaches the local minimum. A fast jump back to the left branch under (13)–(14) then ensues, followed by slow evolution under (11)–(12) along the left branch back to the local maximum.

When the  $AB$  to  $INT1$  inhibition is present ( $g_{AB \rightarrow I} > 0$ ), then a portion of the  $V_L$  nullcline moves in phase space. In particular, when the  $AB$  to  $INT1$  synapse is active, then  $V_I$  decreases. In turn, through equation (5),  $s_{I \rightarrow L}$  decreases causing the  $V_L$  nullcline to move down in the phase space. However, since the  $AB$  to  $INT1$  synapse is irrelevant when  $LG$  is active, only the left branch of the nullcline is affected. The left panel of Fig. 2B shows the  $LG$  trajectory when the  $AB$  to  $INT1$  inhibition is present. The small depolarizations while the trajectory is on the left branch correspond to periodic disinhibition from the  $INT1$  inhibition to  $LG$  that is itself created by the periodic inhibition of  $INT1$  by  $AB$ . When the trajectory has evolved sufficiently far up the left branch to above the local maximum of the lower nullcline, the disinhibition allows  $LG$  to escape from the  $INT1$  inhibition and become active. In this case, the period of the orbit is reduced since the time spent on both the left and right branches is reduced.

### 3.2 The effect of non-voltage dependent electrical coupling on the $INT$ - $LG$ generated rhythm

We next investigate the effect of adding electrical coupling to the network. First we consider the case when the electrical coupling is not voltage dependent. To do so, set  $v_{el} = -100$ . Since  $V_L > v_{el}$  in this case, this causes  $n_{\infty}(V_L) = 1$  in equations (9)–(10). The effect of  $\bar{g}_{elec} > 0$  is to lower the  $V_L$  nullcline in the phase space; see Fig. 3A. Note that because  $V_M$  does not change and, for this case  $g_{elec}(V_L)$  is constant, the effect of the electrical current on the  $V_L$  nullcline is largely due to the difference  $V_L - V_M$ . This difference is the driving force of the electrical current. Since  $V_M$  is constant, it acts like the driving force of a synaptic current that drives the voltage towards a constant reversal potential. When  $\bar{g}_{elec} > 0$ , the left branch of the  $V_L$ -nullcline moves down more than the right branch since the driving force is larger there. That being said, the effect on the left branch is not too much larger than on the right branch. The result of the electrical coupling is simply to increase the burst duration of  $LG$  and shorten its interburst duration. The reason for this is readily explained through the phase plane of  $LG$ . The slow flow is directly related to the distance of the trajectory from the  $s$ -nullcline. When  $\bar{g}_{elec} > 0$ , the right branch of the nullcline moves down toward  $s = 0$  thereby

slowing the trajectory down when  $LG$  is active. The opposite happens to the left branch; the distance from the  $s$ -nullcline increases, thus speeding up the trajectory in the silent state. The period of  $LG$  is an increasing function of  $\bar{g}_{elec}$ . In fact, the period tends to infinity when  $\bar{g}_{elec}$  becomes sufficiently large as a saddle-node bifurcation at  $s = 0$  is created.

Next, observe that electrical coupling and the MCN1 synapse have similar effects on the  $V_L$ -nullcline. Namely, increases in either  $g_{M \rightarrow L}$  or  $\bar{g}_{elec}$  lower the  $V_L$  nullcline. This implies that some amount of the chemical synaptic excitation can be replaced by the metabolically less costly electrical coupling. For instance, begin with  $\bar{g}_{elec} = 0$  and  $g_{M \rightarrow L}$  chosen such that the left branch of the  $V_L$ -nullcline intersects  $s = 1$  creating a stable fixed point; Fig 3B. If  $\bar{g}_{elec}$  is now chosen sufficiently large then the  $V_L$ -nullcline is lowered enough so that the fixed point on the left branch moves to the middle branch and is unstable. However, if  $\bar{g}_{elec}$  is too large, then the right branch of the  $V_L$ -nullcline intersects the  $s$ -nullcline at  $s = 0$  creating an asymptotically stable fixed point there. Thus, there can exist a range  $(\bar{g}^*(g_{M \rightarrow L}), \bar{g}^*(g_{M \rightarrow L}))$  of  $\bar{g}_{elec}$  values for which the fixed point lies along the middle branch and oscillations can occur. Note however if  $g_{M \rightarrow L}$  is too small, then the value  $\bar{g}_{elec}$  needed to move the local maximum below  $s = 1$  would be so large that it would also lower the local minimum to below  $s = 0$ , creating a stable fixed point there. In these cases there is no range of  $\bar{g}_{elec}$  values that produce oscillations.

We can get a better understanding of the range of conductance values for which oscillations exist. Figure 3C shows a bifurcation diagram in  $g_{M \rightarrow L}$ - $\bar{g}_{elec}$  space for the non-voltage dependent case. The shaded region  $R1$  depicts the range of parameter values for which oscillations exist. Note that this region is bounded on three sides by lines. The lower boundary along  $\bar{g}_{elec} = 0$  corresponds to the range of oscillations that exist when there is no electrical coupling. For this set of parameters, the boundary begins at roughly  $(8.91, 0)$ . If  $g_{M \rightarrow L} < 8.91$  and  $\bar{g}_{elec} = 0$ , then there are no oscillations as the  $V_L$ -nullcline has a fixed point on its left branch at  $s = 1$ .

The left boundary corresponds to the set of saddle-node values along the local maximum of the  $V_L$ -nullcline at  $s = 1$ . This curve is a line and has negative slope. To see why, consider the equation  $F(V_L, s) = 0$  and equation (15) for the  $V_L$  nullcline in the voltage independent case where  $g_{elec}(V_L) = \bar{g}_{elec}$ . We rewrite (15) as follows

$$s = \frac{f(V_L) - \bar{g}_{elec}[V_L - V_M]}{g_{M \rightarrow L}[V_L - E_{exc}]}, \quad (16)$$

where  $f(V_L)$  refers to the first two terms in the numerator on the left hand side of (15). A saddle-node point occurs when  $F(V_L, 1) = 0$  and  $ds/dV_L = 0$ . The equation  $F(V_L, 1) = 0$  implies

$$\bar{g}_{elec} = -\frac{V_L - E_{exc}}{V_L - V_M} g_{M \rightarrow L} + \frac{f(V_L)}{V_L - V_M}. \quad (17)$$



Next observe that

$$\frac{ds}{dV_L} = \frac{[df/dV_L - \bar{g}_{elec}][V_L - E_{exc}] - [f(V_L) - \bar{g}_{elec}[V_L - V_M]]}{g_{M \rightarrow L}[V_L - E_{exc}]^2}. \quad (18)$$

The condition  $ds/dV_L = 0$  implies that the numerator of the above fraction equals zero which reduces to the relationship,

$$\frac{df}{dV_L}[V_L - E_{exc}] - f(V_L) - \bar{g}_{elec}[V_M - E_{exc}] = 0. \quad (19)$$

Let  $V_L^*(\bar{g}_{elec})$  denote the solution of (19) and note it that does not depend on  $g_{M \rightarrow L}$ . Further, it only weakly depends on  $\bar{g}_{elec}$  in the sense that this term is scaled by the difference  $V_M - E_{exc}$ . Therefore the curve that defines the saddle-node points given in (17) is basically a line with the slope given by the ratio of the driving forces  $(V_L^* - E_{exc})/(V_L^* - V_M)$ . Note that if  $E_{exc} = V_M$ , then the slope of the saddle-node curve is negative one and the  $V_L^*$  value of the local maximum is independent of both  $g_{M \rightarrow L}$  and  $\bar{g}_{elec}$ .

The top boundary of the oscillation region corresponds to the set of saddle-node points when the minimum of the cubic nullcline is tangent to  $s = 0$ . This curve is given by  $F(V_L, 0) = 0$  and  $ds/dV_L = 0$ . From (19), we already know that the solution to the latter are independent of  $g_{M \rightarrow L}$ . Now from (16), the intersection of the  $V_L$  nullcline with  $s = 0$  is also independent of  $g_{M \rightarrow L}$ . Thus the top boundary is simply a horizontal line in the  $g_{M \rightarrow L} - \bar{g}_{elec}$  plane.

The region  $R1$  is unbounded on the right. This is precisely because the local minimum of  $s$  at  $s = 0$  is independent of  $g_{M \rightarrow L}$ . As  $g_{M \rightarrow L} \rightarrow \infty$ , the oscillations are no longer burst-like. Instead the trajectory spends almost all of its time on the right branch in a neighborhood of the local minimum.

### 3.3 The effect of voltage dependent electrical coupling on the *INT1* – *LG* generated rhythm

To explore the role of voltage dependence on the electrical coupling in the *INT1-LG* generated rhythm, we let  $v_{el} = V_T$  which is a value that lies along the middle branch of the  $V_L$ -nullcline. The voltage dependence now allows the conductance of the electrical coupling to vary as a function of  $V_L$  between  $g_{min}$  along the left branch of the  $V_L$ -nullcline and  $\bar{g}_{elec}$  along the right branch. Thus the voltage-dependent electrical coupling affects the right branch of the  $V_L$  nullcline much more than the left branch. This is in contrast to the non-voltage dependent case; compare Fig 4A and B.

Figure 4C shows the regions of oscillations for these cases. For this set of parameters, there are two primary differences between the voltage-dependent ( $R2$ ) and independent ( $R1$ ) cases. First, the left boundary is more steeply sloped and the top boundary sits at a higher

$\bar{g}_{elec}$  value compared to the voltage-independent case. Both are easily explained. In the voltage-dependent case, equation (17) becomes

$$\bar{g}_{elec} = -\frac{V_L - E_{exc}}{n_\infty(V_L)[V_L - V_M]} g_{M \rightarrow L} + \frac{f(V_L)}{V_L - V_M}. \quad (20)$$

The condition  $ds/dV_L = 0$  yields a solutions  $V_L^*(\bar{g}_{elec})$  which is again independent of  $g_{M \rightarrow L}$ . By definition  $n_\infty(V_L) < 1$ . Thus the prefactor multiplying  $g_{M \rightarrow L}$  is in fact a slope and is larger in magnitude than in the voltage-independent case. Thus the left boundary is steeper ( $-5.4$  compared to  $-0.8$  for the default parameters).

The intersection of the  $V_L$  nullcline with  $s = 0$  satisfies

$$\bar{g}_{elec} n_\infty(V_L^{**}) = \frac{g_{rest,L} [V_L^{**} - E_{rest,L}] + g_{I \rightarrow L} s_{I \rightarrow L} (h_1(V_L^{**}, s_{AB \rightarrow I})) [V_L^{**} - E_{inh}]}{V_M - V_L^{**}}. \quad (21)$$

The value  $V_L^{**}$  increases with voltage dependence (specifically with  $v_{el}$  from (10)). As a result, the right-hand side of (21) increases since the numerator increases while the denominator decreases. In the voltage independent case,  $n_\infty(V_L) \equiv 1$ , whereas in the voltage dependent case  $n_\infty(V_L^{**}) < 1$ . To compensate, the maximal conductance of the electrical coupling  $\bar{g}_{elec}$  must increase. This allows the top boundary of the region  $R2$  to sit at higher values of  $\bar{g}_{elec}$  ( $\approx 1.57$  compared to  $1.2$  in the voltage independent case).

The effect of voltage dependence can be amplified by making the  $n_\infty(V_L)$  curve less steeply sloped. For instance, if  $k_{el}$  is increased from 5 to 20, then the slope of the left boundary of the oscillation region decreases in magnitude to around 2, which is much closer to the voltage-independent case; see  $R3$  in Fig. 4D. Further, because the change in  $n_\infty$  is more gradual, larger values of  $\bar{g}_{elec}$  are needed to satisfy (21), so that the top boundary of  $R3$  now sits around 2.02 compared to 1.57 for  $R2$ . Other changes of parameters can similarly be explored.

### 3.4 Oscillations arising through the voltage-dependent $MCM1-LG$ coupling in the absence of the $INT1-LG$ HCO

To this point, we have simply shown how electrical coupling affects the existing oscillations that arise through the  $INT1-LG$  HCO. A more important observation that we now make is that oscillations can arise in the absence of this HCO provided that the electrical coupling is voltage-dependent.

Consider equations (11)–(14) with  $g_{I \rightarrow L} = 0$ . This removes the  $INT1$  to  $LG$  inhibition and destroys the HCO mechanism for oscillations. The  $V_L$ -nullcline now is defined by

$$s = \frac{-g_{rest,L}[V_L - E_{rest,L}] - \bar{g}_{elec} n_\infty(V_L)[V_L - V_M]}{g_{M \rightarrow L}[V_L - E_{exc}]}. \quad (22)$$

In this case, to see why voltage dependence is necessary for oscillations, first take the case where the electrical coupling is non-voltage dependent. Then  $ds/dV_L = [g_{rest,L}[E_{exc} - E_{rest,L}] + \bar{g}_{elec}[E_{exc} - V_M]]/g_{M \rightarrow L}[V_L - E_{exc}]^2 > 0$  if  $V_M$  is not too large. In this case, the  $V_L$  nullcline is a monotone increasing function that asymptotes to  $-[g_{rest,L} + \bar{g}_{elec}]/g_{M \rightarrow L}$  as  $V_L \rightarrow -\infty$  and  $E_{exc}$  as  $V_L \rightarrow \infty$ ; see Fig 5A. In this case, oscillations are not possible as any ensuing fixed point is asymptotically stable.

Now take the case when the electrical coupling is voltage dependent. Then after some algebraic manipulation, the condition  $ds/dV_L = 0$  yields

$$g_{rest,L}[E_{exc} - E_{rest,L}] = \bar{g}_{elec} \left[ \frac{dn_\infty}{dV_L}[v_L - E_{exc}]^2 + [V_L + n_\infty(V_L) - E_{exc}][V_M - E_{exc}] \right].$$

For simplicity, take  $E_{exc} = V_M$  in which case the condition reduces to

$$g_{rest,L}[V_M - E_{rest,L}] = \bar{g}_{elec} \frac{dn_\infty}{dV_L}[V_L - V_M]^2. \quad (23)$$

The left hand side is independent of  $\bar{g}_{elec}$ , while the right hand side increases with it. Further the right hand side has a zero at  $V_L = V_M$  and also tends to 0 as  $V_L \rightarrow \pm\infty$ . Thus for  $\bar{g}_{elec}$  sufficiently large, there are two solutions of (23), meaning that the graph of (22) has a local maximum and minimum. In this case, the  $V_L$ -nullcline is again cubic shaped and oscillations are possible; see Fig 5B black trajectory and voltage trace. Therefore, voltage-dependent electrical coupling together with the slow excitation from MCN1, and its subsequent removal, via pre-synaptic inhibition from *LG* provides an alternate mechanism for the generation of oscillations. Note that the voltage range and period of the oscillation are within the range of the oscillation generated by the *INT1 - LGHCO*.

Using equation (10), we can derive an estimate on how large  $\bar{g}_{elec}$  needs to be to obtain oscillations. The right hand side of (23) has a local maximum at  $V_L = V_{el}$ . Substituting and finding the smallest value of  $\bar{g}_{elec}$  that allows the right hand side to equal the left yields

$$\bar{g}_{elec} \geq \frac{4g_{rest,L} k_{el}[V_M - E_{rest,L}]}{[v_{el} - V_M]^2}. \quad (24)$$

This condition is fairly straightforward to interpret. Namely, the stronger the passive properties of *LG*, either through larger leak conductance  $g_{rest,L}$  or smaller leak reversal

$E_{rest,L}$ , or the more gradual the voltage dependence, larger  $k_{el}$  or  $v_{el}$ , the larger the electrical conductance  $\bar{g}_{elec}$  needs to be.

We next explore the role of *INT1* on the *MCM1* – *LG* generated oscillation. We emphasize that, although the inhibition from *INT1* to *LG* is restored, the parameters remain in range where the inhibition based HCO-based mechanism is not capable of producing oscillations. *INT1* inhibition to *LG* raises the LB of  $V_L$ -nullcline as shown in Fig 5B. Now the trajectory (black) must increase to higher values of  $s$  in the phase plane to escape inhibition, thereby increasing the interburst duration. In turn, when *LG* is active, the trajectory must also traverse through a larger range of  $s$  values to reach the local minimum of the cubic, thereby increasing *LG*'s burst duration. Thus the effect of this inhibition is to increase the oscillation period (and range of voltage values) by increasing both the interburst and burst duration (black voltage traces).

When *AB* to *INT1* inhibition is included, the trajectory is allowed to leave the left branch prematurely at one of the moments in time when *INT1* is inhibited by *AB*. This results in a shorter interburst and burst duration very similar to what was described in Section 3.1. Note that the period is very similar to that obtained when *INT1* to *LG* inhibition is completely absent ( $g_{I \rightarrow L} = 0$ ); see Fig. 5C. This makes sense as the *AB* inhibition to *INT1* has the practical effect of making  $g_{I \rightarrow L} = 0$  periodically when *LG* is in its interburst. Thus it is at one of those moments in time when *LG* is able to escape from inhibition.

### 3.5 Voltage-dependent oscillations in the Morris-Lecar equations

We now demonstrate that our main findings regarding the role of voltage dependent electrical coupling hold in a model in which *LG* and *INT1* are modeled using biophysical equations. We model each of these cells using the two-dimensional Morris-Lecar equations, which are a commonly used set of equations that are derived in the Hodgkin-Huxley formalism. The voltage equation includes ionic currents for calcium, potassium and a leak current. There is a recovery variable associated with the activation of the potassium current. The equations for each cell are

$$\begin{aligned} \varepsilon \frac{dV_L}{dt} = & -g_{leak,L} [V_L \\ & - E_{leak,L}] - g_{Ca,L} m_\infty(V_L) [V_L - E_{Ca}] - g_K w_L [V_L \\ & - E_K] - I_{syn,I \rightarrow L}(V_I, V_L) - I_{syn,M \rightarrow L}(V_M, V_L, s) \\ & - I_{elec}(V_L, V_M) + I_{app,L} \end{aligned} \quad (25)$$

$$\frac{dW_L}{dt} = \phi_L [w_{\infty,L}(V_L) - W_L] / \tau_\infty(V_L) \quad (26)$$

$$\varepsilon \frac{dV_I}{dt} = -g_{leak,I} [V_I - E_{leak,I}] - g_{Ca,I} m_\infty(V_I) [V_I - E_{Ca}] - g_K w_I [V_I - E_K] - I_{syn,L \rightarrow I}(V_I, V_L) - I_{syn,AB \rightarrow I}(V_I, s_{AB \rightarrow I}) + I_{app,I} \quad (27)$$

$$\frac{dW_I}{dt} = \phi_I [w_{\infty,I}(V_I) - W_I] / \tau_\infty(V_I). \quad (28)$$

On the right-hand side of equations (25) and (27), the first three terms are specific to the Morris-Lecar equations, while the remaining terms have the same form as defined in Section 2.1. The specific details of the model and parameter values are provided in the Appendix. Of interest to us here is the shape of the nullclines of the two cells. For *INT1*, parameters are chosen such that in the absence of input ( $g_{L \rightarrow I} = 0$ ,  $g_{AB \rightarrow I} = 0$ ), the  $V_I$  nullcline is cubic shaped and intersects the sigmoidal  $W_I$  nullcline on its right branch. This high voltage fixed point indicates that *INT1* is tonically active in the absence of input.

For *LG*, we consider two different parameter choices. In one case, in the absence of input, we choose  $g_{Ca,L} = 4.0$  which is large enough so that the  $V_L$  nullcline is cubic shaped. In that case, the  $V_L$  and  $W_L$  nullclines intersect along the left branch of  $V_L$  which models *LG* being at rest. In this case, *LG* is excitable in the classical sense that, if it receives the appropriate synaptic input from *MCN1*, it will fire. With these parameters, and with the *LG-INT1* HCO intact, the presynaptic *LG* to *MCN1* inhibition is sufficient to produce oscillations, as was shown in the previous sections. The addition of electrical coupling, either voltage-dependent or not, simply modulates the oscillations in a manner analogous to that found in Sections 3.2 and 3.3. In other words, electrical coupling is not necessary to produce oscillations. Numerical simulations (not shown) in this case yield results that are qualitatively similar to those found in Figs. 3 and 4.

The more interesting situation arises in the second case when we choose  $g_{Ca,L} = 0.5$  so that the  $V_L$  nullcline is monotone decreasing. Now, *LG* is no longer excitable. As a result, the *INT1-LG* HCO is not able to produce oscillations, independent of whether  $g_{I \rightarrow L}$  is zero or not. Just as in Section 3.4 with the simple model, voltage dependent electrical coupling can provide an alternative mechanism for oscillations. Figure 6 shows results from the biophysical model. First consider the case when  $g_{I \rightarrow L} = 0$ . The phase plane in Fig. 6A shows the projection of  $V_L$  nullcline for four different cases onto the  $V_L - W_L$  phase plane when the electrical coupling is independent of voltage. The solid curves are for  $\bar{g}_{elec} = 2.2$  where brown corresponds to  $s = 0$  and red is  $s = 1$ . The dashed curves are their counterparts for  $\bar{g}_{elec} = 22$ . Because the *MCN1* to *LG* excitation which is governed by  $s$  can change slowly, the four nullclines that are shown are only representative snapshots of the  $V_L$  nullcline. However for all values of  $s$ , the  $V_L$  nullcline is monotone decreasing, precluding the possibility of oscillations.

In contrast, consider Fig. 6B1. Shown is the  $V_L$  nullcline when the electrical coupling is voltage-dependent for two different values of  $s$  (smaller  $s$  in brown, larger in red). As can be seen, the voltage dependence creates a cubic shaped nullcline by preferentially affecting the nullcline at higher voltages. As a result oscillations are possible. The  $V_L$  trajectory is superimposed on the figure. The red nullcline associated with the larger value of  $s$  corresponds to those at which the trajectory jumps from the left branch to the right branch signaling  $LG$ 's transition to the active state. The brown nullcline is associated with a smaller value of  $s$  when the  $LG$  trajectory jumps from the right branch to the left branch signaling  $LG$ 's transition to the silent state. The dependence on  $s$  is seen in panel B2 which shows the projection of nullclines and the trajectory onto the  $V_L$  versus  $s$  phase space; note the parallel to Fig. 5B. Recall that  $s$  increases when  $LG$  is in the silent phase. This means that in the  $V_L - s$  phase plane, the trajectory moves up along the left branches. However, the left branches themselves are moving down because as  $s$  increases, the added excitation from  $MCM$  produces a greater chance to become active. The jump to the active state occurs from a local maximum of the red nullcline. On the right branch, the trajectory moves down, but the nullcline moves up. The jump to the silent state occurs from the minimum of the brown nullcline. The corresponding voltage traces for both  $LG$  and  $INT1$  are shown in panel B3.

In Fig. 6C, we restore the  $INT1$  to  $LG$  synapse  $g_{I \rightarrow L} = 10$ . The  $LG$  interburst length increases, as was also seen in the simple model Fig. 5B. As before, this is because the inhibition from  $INT1$  to  $LG$  means that  $s$  has to increase to larger values for  $LG$  to jump to the active state. This implies a longer interburst duration. Finally, in Fig. 6C, we restore the  $AB$  input to  $INT1$  which shortens the  $LG$  burst and interburst in a similar manner to Fig. 5C because the periodic inhibition of  $INT1$  by  $AB$  provides periodic disinhibition of  $LG$ . This provides  $LG$  an opportunity to escape the silent state earlier just as with the simple model, thereby shortening  $LG$ 's interburst and speeding up the rhythm.

Just as in Section 3.4, we can determine conditions under which voltage-dependence allows the electrical coupling to produce oscillations. Consider the case  $g_{I \rightarrow L} = 0$ . For compactness of notation, define  $f(V_L) = -g_{rest,L}[V_L - E_{rest,L}] - g_{Ca,L}m_\infty(V_L)[V_L - E_{Ca}]$ ,  $h(V_L) = -\bar{g}_{elec}n_\infty(V_L)[V_L - E_M] - g_s s[V_L - E_{exc}] + I_{app,L}$ . Note that  $s$  depends on  $V_L$ . Let prime denote the derivative with respect to  $V_L$ . We can solve for the  $V_L$  nullcline by setting the right-hand side of equation (25) to zero and solving for  $W_L$ .

$$W_L = \frac{f(V_L) + h(V_L)}{g_K[V_L - E_K]} \quad (29)$$

The slope of this nullcline is given by

$$\frac{dW_L}{dV_L} = \frac{[f'(V_L) + h'(V_L)][V_L - E_K] - [f(V_L) + h(V_L)]}{g_K[V_L - E_K]^2} \quad (30)$$

To show that the  $V_L$  nullcline can be cubic shaped, we need to find conditions under which the derivative (29) changes sign. Observe that  $f(V_L) + h(V_L) > 0$  thus the second term in the numerator of (30) is negative. Next observe that

$$f'(V_L) = -g_{rest,L} - g_{Ca,L} [m'_\infty(V_L)[V_L - E_{Ca}] + m_\infty(V_L)] < 0 \quad (31)$$

if  $g_{Ca,L}$  is sufficiently small. The derivative

$$h'(V_L) = -\bar{g}_{elec} n'_\infty(V_L)[V_L - V_M] - \bar{g}_{elec} n_\infty(V_L) - g_s s' [V_L - E_{exc}] - g_{ss}. \quad (32)$$

The first term in (32) is non-negative, while the remaining three are all negative (note that  $s'(V_L) < 0$ ). Thus the sign of  $h'(V_L)$  will be negative unless the first term is sufficiently large. When the electrical coupling is not dependent on voltage,  $n_\infty(V_L) \equiv 1$  and therefore  $n'_\infty(V_L) = 0$ . Thus the first term will actually be zero in this case. In turn this implies that  $h'(V_L) < 0$ . Together, these results imply that, in the voltage-independent case, the  $V_L$  nullcline remains monotone decreasing and that no oscillations are possible. Alternatively, when the electrical coupling is voltage dependent, then  $n'_\infty(V_L) > 0$  and is also relatively large in an intermediate range of  $V_L$  values (roughly  $-35$  to  $-15$  mv). Thus for  $\bar{g}_{elec}$  sufficiently large, the first term in (32) dominates the others and  $h'(V_L) > 0$ . As a consequence, if  $\bar{g}_{elec}$  is large enough, then voltage dependent electrical coupling allows  $dW_L/dV_L > 0$  over a range of intermediate  $V_L$  values. In conjunction with the synaptic input from *MCNI*, this provides the opportunity for oscillations to exist.

## 4 Discussion

Neuronal circuits involved in the generation of rhythmic behavior often involve half center oscillators that are composed of sets of reciprocally inhibitory neurons. There is an extensive and ongoing effort to understand the dynamics of half center oscillators in the context of central pattern generation [10, 11, 14, 16, 17]. In many cases, it has been noted that a careful coordination between network elements is necessary to generate and set the frequency of the network [18, 19, 20]. The role of electrical coupling in rhythmic networks has also been studied [21, 22] where the neurons were modeled as intrinsic oscillators. Electrical coupling was not needed to generate oscillations, but rather used to modulate the characteristics of the oscillation.

As part of a larger work on the role of feedback to projection neurons, Kintos and colleagues [10, 12] had shown how to employ phase plane analysis to understand the effect of *MCNI* synaptic input on the *GMR*. In particular, they showed how to analyze *MCNI* synaptic input and *AB* inhibition of *INT1* to determine the frequency of the *GMR*. In this paper, we have extended this analysis to show how to incorporate the effect of *MCNI* – *LG* voltage-dependent electrical coupling to determine the conditions under which electrical coupling in the absence of the *LG* – *INT1* HCO can generate oscillations.

In the presence of an intact  $LG-INT1$  HCO, we first considered the effect of non-voltage dependent electrical coupling. We showed that the non-voltage dependent electrical coupling acts to increase the  $LG$  burst duration while shortening its interburst duration. This occurs because the voltage of  $LG$  is driven towards the fixed, large voltage of  $MCM1$ . If the strength of the electrical coupling is too large, however,  $LG$  gets stuck in its burst phase. One advantage of the non-voltage dependent electrical coupling is that it can be used in conjunction with the  $MCM1$  chemical synapse allowing for the generation of the  $GMR$  for a smaller amount of the chemical excitation. This is a "cheaper" way to generate oscillations as it requires less synaptic resources. The bifurcation diagram in Fig. 3C shows the precise relationship between electrical and synaptic coupling needed to create oscillations. We showed that boundaries of this diagram are all roughly linear. In the case of voltage dependent electrical coupling, the right branch of the  $LG$  nullcline is affected much more significantly than the left branch. This allows for an increase in the  $LG$  burst duration and a larger range of values of  $\bar{g}_{elec}$  for the generation of network oscillations.

A significant finding of our study is that network oscillations can also be generated in the absence of coupling between  $LG$  and  $INT1$  simply through the voltage dependent electrical coupling between  $MCM1$  and  $LG$  and the slow excitation from  $MCM1$ , together with its removal due to the pre-synaptic inhibition of this excitation. We derived a condition on the minimum value of  $\bar{g}_{elec}$  in order for the  $GMR$  oscillations to exist in the absence of the HCO. We showed that non-voltage dependent electrical coupling alone is not sufficient for generation of the  $GMR$ . When the reciprocal inhibition between  $LG$  and  $INT1$  is restored, the period of the oscillations increases due to increases in both the interburst and burst durations of the oscillations. If, in addition,  $AB$  periodically inhibits  $INT1$ , the interburst duration of  $LG$  is shortened. This is a direct result of the disinhibitory effect of  $LG$  from  $INT1$  each time  $AB$  fires.

Our findings are not limited to the simple model in which  $LG$  and  $INT1$  are modeled as passive cells that we first considered. We showed that voltage-dependent electrical coupling played the same role in a model in which these cells were described using the biophysically based Morris-Lecar equations. In order for voltage-dependent electrical coupling to create the mechanism for oscillations, we showed that  $LG$  must not be modeled as being excitable. This fact is consistent with the underlying biological properties of the  $LG$  neuron, which, in the absence of  $MCM1$  or other modulatory input, shows no active properties (e.g. post-inhibitory rebound, voltage sags or plateaus) that are associated with slow bursting oscillations [4].

There are several natural extensions of this work. In previous work [23], based on experiments of Wood et. al. [24], we showed that  $AB$  inhibition to  $MCM1$  provides an alternate mechanism to regulate the gastric mill frequency. In the current work, we did not include the inhibition from  $AB$  to  $MCM1$ . If the  $AB$  inhibition to  $MCM1$  were included, the  $LG$  burst would end when  $AB$  inhibits  $MCM1$ . It would be necessary for  $MCM1$  to be gated when  $LG$  is in its active state in order to maintain robust oscillations. Indeed, in the VCN-activated version of the gastric mill rhythm, the  $AB$  to  $MCM1$  synapse is gated out during  $LG$  active phase [25]. It would be of interest to extend our current model to test whether this gating is truly necessary to maintain oscillations.



Another area that remains to be explored is the role of electrical coupling in the *MCN1/CP N2* generated gastric mill rhythm. Kintos and Nadim [10] showed that the *LG – INT1 HCO* could be replaced by a tri-synaptic pathway that included the projection neuron *CP N2*. Of interest would be to see whether voltage dependence can replace one or more of those synaptic pathways.

Although the networks under consideration in this, and related papers, are relatively simple and only involve a small number of neurons, it is evident that the dynamics exhibited by them can be quite complicated. Moreover, the neural mechanisms that underlie the existence of oscillations are often hard to separate from those that simply modulate the rhythmic properties of these networks. Minimal modeling and mathematical analysis of small networks plays a critical role in allowing us to discern which inputs generate oscillations versus those that modulate oscillations by providing valuable insights into how these important central pattern generating networks operate.

## Acknowledgments

This work was supported in part by the National Science Foundation, DMS 1122291 (AB, FN) and the National Institutes of Health, NIH R01-MH060605 (FN).

## List of Abbreviations

<b>CPG</b>	central pattern generating
<b>GMR</b>	gastric mill rhythm
<b>STG</b>	stomatogastric ganglion
<b>HCO</b>	half-center oscillator
<b>LG</b>	lateral gastric
<b>INT1</b>	interneuron 1
<b>STNS</b>	stomatogastric nervous system
<b>AB</b>	anterior burster
<b>MCN1</b>	modulatory commissural neuron 1

## References

1. Sneyd J, Keizer J, Sanderson MJ. Mechanisms calcium oscillations and waves: a quantitative analysis. *The FASEB Journal*. 1995; 9(14):1463–1472. [PubMed: 7589988]
2. Marder E, Bucher D. Central pattern generators and the control of rhythmic movements. *Current Biology*. 11(23):R986–R996. [PubMed: 11728329]
3. Nusbaum MP, Beenhakker MP. A small-systems approach to motor pattern generation. *Nature*. 2002; 417:343–350. [PubMed: 12015615]
4. Coleman M, Nusbaum MP. Functional consequences of compartmentalization of synaptic input. *Journal of Neuroscience*. 1994; 14:6544–6552. [PubMed: 7965058]
5. Coleman M, Meyrand P, Nusbaum MP. A switch between two modes of synaptic transmission mediated by presynaptic inhibition. *Nature*. 1995; 378:502–505. [PubMed: 7477408]

6. Calabrese RL. Oscillations in motor pattern-generating networks. *Current Opinion Neurobiology*. 1995; 5:816–823.
7. Skinner F, Kopell N, Marder E. Mechanisms for oscillation and frequency control in reciprocally inhibitory model neural networks. *Journal of Computational Neuroscience*. 1994; 1(1–2):69–87. [PubMed: 8792226]
8. Nadim F, Manor Y, Nusbaum MP, Marder E. Frequency regulation of a slow rhythm by a fast periodic input. *Journal of Neuroscience*. 1998; 18:5053–5067. [PubMed: 9634571]
9. Ambrosio C, Bose A, Nadim F. The effect of modulatory neuronal input on gastric mill frequency. *Neurocomputing*. 2005; 65–66:626–631.
10. Kintos N, Nadim F. A Modeling exploration of how synaptic feedback to descending projection neurons shapes the activity of an oscillatory network. *SIAM J Applied Dynamical Systems*. 2014; 13(3):1239–1269.
11. Kintos N, Nusbaum MP, Nadim F. A Modeling comparison of projection neuron-and neuromodulator-elicited oscillations in a central pattern generator network. *J Comput Neurosci*. 2008; 24:374–97. [PubMed: 18046635]
12. Kintos N, Nusbaum MP, Nadim F. A Modeling comparison of projection neuron-and neuromodulator-elicited oscillations in a central pattern generator network. *J Comput Neurosci*. 2016; 40:113–135. [PubMed: 26798029]
13. Manor Y, Nadim F, Epstein S, Ritt J, Marder E, Kopel N. Network oscillations generated by balancing graded asymmetric reciprocal inhibition in passive neurons. *Journal of Neuroscience*. 1999; 19(7):2765–2779. [PubMed: 10087088]
14. Reyes M, Carelli P, Sartorelli J, Pinto R. A modeling approach on why simple central pattern generators are built of irregular neurons. *PLoS ONE*. 2015; 10(3):e0120314. [PubMed: 25799556]
15. Morris C, Lecar H. Voltage oscillations in the barnacle giant muscle fiber. *Biophys J*. 1981; 35:193–213. [PubMed: 7260316]
16. Weeks J. Neuronal basis of leech swimming. *Journal of Neuroscience*. 1981; 45(4):698–723.
17. Zhang C, Lewis T. Phase response properties of half-center oscillators. *Journal of Computational Neuroscience*. 2013; 35(1):55–74. [PubMed: 23456595]
18. Cymbalyuk G, Gaudry Q, Masion M, Calabrese R. Bursting in leech heart interneurons: cell-autonomous and network-based mechanisms. *J Neurosci*. 2002; 22(24):10580–10592. [PubMed: 12486150]
19. Matveev V, Bose A, Nadim F. Capturing the bursting dynamics of a two-cell inhibitory network using a one-dimensional map. *J Comput Neurosci*. 2007; 23(2):169–187. [PubMed: 17440801]
20. Szucs A, Selverston A. Consistent dynamics suggests tight regulation of biophysical parameters in a small network of bursting neurons. *J Neurobiol*. 2006; 66(14):1584–1601. [PubMed: 17058195]
21. Chow C, Kopell N. Dynamics of spiking neurons with electrical coupling. *Neur Comp*. 2000; 12:1643–1678.
22. Lee E, Terman D. Stable antiphase oscillations in a network of electrically coupled model neurons. *SIAM J Appl Dyn Syst*. 2013; 12(1):1–27.
23. Ambrosio-Mouser C, Farzan N, Bose A. The effects of varying the timing of inputs on a neural oscillator. *SIAM Journal on Applied Dynamical Systems*. 2006; 5(1):108–139. [PubMed: 21052553]
24. Wood D, Stein W, Nusbaum M. Projection neurons with shared cotransmitters elicit different motor patterns from the same neural circuit. *J Neuroscience*. 2008; 20(23):8943–8953. [PubMed: 11102505]
25. Blitz DM, Nusbaum MP. State-dependent presynaptic inhibition regulates central pattern generator feedback to descending inputs. *J Neurosci*. 2008; 28:9564–9674. [PubMed: 18799688]
26. Ermentrout, B. *Simulating, analyzing, and animating dynamical systems : a guide to XPPAUT for researchers and students*. Society for Industrial and Applied Mathematics; Philadelphia: 2002.

## 5 Appendix

Numerical simulations were performed using XPPAUT [26]. For the simple model of passive cells used to produce Figs. 2–5 the following set of equations was used.

$$\frac{dV_L}{dt} = -g_{rest,L} [V_L - E_{rest,L}] - g_{M \rightarrow L} s [V_L - E_{exc}] - g_{elec}(V_L) [V_L - V_M] - g_{I \rightarrow L} s_{I \rightarrow L} (h_1(V_L, s_{AB \rightarrow I})) [V_L - E_{inh}] \quad (33)$$

$$\frac{ds}{dt} = \frac{1-s}{\tau_r} Heav(V_T - V_L) - \frac{s}{\tau_f} Heav(V_L - V_T) \quad (34)$$

The term  $V_I = h_1(V_L, s_{AB \rightarrow I})$  that appears in equation (33) is governed by

$$h_1(V_L, s_{AB \rightarrow I}) = \frac{E_{rest,I} + \frac{g_{I \rightarrow I} s_{L \rightarrow I}(V_L) E_{inh} + \frac{g_{AB \rightarrow I} s_{AB \rightarrow I}(t) P(V_L) E_{inh}}{g_{rest,I}}}{1 + \frac{g_{AB \rightarrow I} s_{AB \rightarrow I}(t) P(V_L) + \frac{g_{I \rightarrow I} s_{L \rightarrow I}(V_L)}{g_{rest,I}}}$$

Note here the presence of the function  $P(V_L) = (1 + \exp(\frac{V_L - v_3}{k_3}))^{-1}$ . This term is used to gate out the effect of  $AB$  input to  $INT1$ , and its subsequent effect on the  $V_L$  nullcline when  $INT1$  is in its silent state. The other remaining equations are simply (3–5)

$$s_{AB \rightarrow I}(t) = Heav(\frac{\sin(2\pi t)}{1000} - 0.5), \quad s_{L \rightarrow I}(V_L) = (1 + \exp(\frac{v_1 - V_L}{k_1}))^{-1}, \quad s_{I \rightarrow L}(V_I) = (1 + \exp(\frac{v_2 - V_I}{k_2}))^{-1}$$

and (9) and (10) written as one  $g_{elec}(V_L) = \bar{g}_{elec} [(1 - g_{min})(1 + \exp(\frac{v_{el} - V_L}{k_{el}}))^{-1} + g_{min}]$ .

Table 1 shows parameter values that were common to all simulations of the simple model. Below that we show specific values used for  $\bar{g}_{elec}$  and  $g_{M \rightarrow L}$  for each of the relevant figures.

For Figures 2 to 4, we chose  $g_{I \rightarrow L} = 12$ . For Figure 2:  $g_{M \rightarrow L} = 10$ ,  $\bar{g}_{elec} = 0$ ,  $g_{AB \rightarrow I} = 0$  (2A) and  $g_{AB \rightarrow I} = 0.2$  (2B). For Figure 3A:  $g_{M \rightarrow L} = 10$ ,  $g_{AB \rightarrow I} = 0$  and  $\bar{g}_{elec} = 0, 0.5, 1.0, 1.5$ . For Figure 3B:  $g_{M \rightarrow L} = 8.8$  and  $\bar{g}_{elec} = 0.0$  (upper cubic) and  $0.8$  (lower cubic). For Figure 4A, the electrical coupling is non-voltage dependent:  $g_{M \rightarrow L} = 8.8$  and  $\bar{g}_{elec} = 0.088$ ,  $\bar{g}_{elec} = 0.155$  at the left saddle node point, and  $\bar{g}_{elec} = 1.2$  at the right saddle node point. For Figure 4B, the electrical coupling is voltage dependent and we chose,  $g_{M \rightarrow L} = 8.8$  and  $\bar{g}_{elec} = 0$ ,  $\bar{g}_{elec} = 0.594$  at the left saddle node point, and  $\bar{g}_{elec} = 1.57$  at the right saddle node point.

For Figure 5A:  $g_{M \rightarrow L} = 0.35$ ,  $g_{I \rightarrow L} = 0$ , the three monotone nullclines are when the electrical coupling is non-voltage dependent with  $\bar{g}_{elec} = 0$ ,  $\bar{g}_{elec} = 0.6$  and  $\bar{g}_{elec} = 1.3$ . The cubic is for the voltage-dependent case with  $\bar{g}_{elec} = 1.3$ . For Figure 5B: voltage dependent electrical coupling,  $g_{M \rightarrow L} = 0.35$ ,  $\bar{g}_{elec} = 1.24$ ,  $g_{I \rightarrow L} = 0$  (lower cubic) or  $g_{I \rightarrow L} = 0.2$  (upper cubic). For Figure 5C: same as Fig. 5B except  $g_{AB \rightarrow I} = 0.2$ .

For the simulations shown in Fig. 6, the following set of equations was used:

$$\begin{aligned}
 C \frac{dV_L}{dt} &= -g_{leak,L} [V_L - E_{leak}] - g_K w_L [V_L - E_K] - g_{Ca,I} m_\infty(V_L) [V_L - E_{Ca}] \\
 &\quad - g_{I \rightarrow L} s_{I \rightarrow L} I [V_L - E_{inh}] - g_s s [V_L - E_{exc}] - g_{elec}(V_L) [V_L - V_M] + I_{app,L} \\
 \frac{dW_L}{dt} &= \phi_L \frac{w_{\infty,L}(V_L) - W_L}{\tau_\infty(V_L)} \\
 C \frac{dV_I}{dt} &= -g_{leak,I} [V_I - E_{leak}] - g_K w_I [V_I - E_K] - g_{Ca,I} m_\infty(V_I) [V_I - E_{Ca}] \\
 &\quad - g_{L \rightarrow I} s_{L \rightarrow I} [V_I - E_{inh}] - g_{AB \rightarrow I} s_{AB}(t) [V_I - E_{sym}] + I_{app,I} \\
 \frac{dW_I}{dt} &= \phi_I \frac{w_{\infty,I}(V_I) - W_I}{\tau_\infty(V_I)}
 \end{aligned}$$

The synaptic variables are governed by

$$\begin{aligned}
 \frac{ds_{I \rightarrow L}}{dt} &= \gamma \left( \frac{1}{1 + \exp\left(\frac{v_{ith} - V_L}{t_\alpha}\right)} - s_{I \rightarrow L} \right) \\
 \frac{ds_{L \rightarrow I}}{dt} &= \alpha (1 - s_{L \rightarrow I}) Heav(V_L - V_T) - \beta s_{L \rightarrow I} Heav(V_T - V_L) \\
 \frac{ds}{dt} &= \frac{1-s}{\tau_r} Heav(V_T - V_L) - \frac{s}{\tau_f} Heav(V_L - V_T).
 \end{aligned}$$

The remaining terms are given by

$m_\infty(V_x) = (1 + \tanh(\frac{V_x - cv1}{cv2}))/2$ ,  $\tau_\infty(V_x) = \cosh(\frac{V_x - cv3}{2cvv})$ ,  $w_{\infty,x}(V_x) = (1 + \tanh(\frac{V_x - wf_x}{cv4}))/2$ ,  
 where the subscript  $x$  refers to either  $L$  or  $I$ . In addition, we used equations (3), (9) and (10).  
 For Fig. 6A–B,  $g_{I \rightarrow L} = 0$ , for Fig. 6C,  $g_{I \rightarrow L} = 10$  and for Fig. 6D,  $g_{AB \rightarrow I} = 1$ . Table 2 shows  
 parameter values for the simulations of the Morris-Lecar model.

### Highlights

- A simple model is used to understand how electrical coupling affects the ability of oscillations to be created through a standard half-center oscillator mechanism is incapable of doing so.
- Voltage-dependent electrical coupling is shown to provide an alternate mechanism for the generation of oscillations when an inhibition based half-center oscillator mechanism is incapable of doing so.
- This same result is then demonstrated in a biophysical model based on the Morris-Lecar equations.
- Conditions on the parameters in both models are derived that show why electrical coupling must be voltage dependent to produce oscillations.

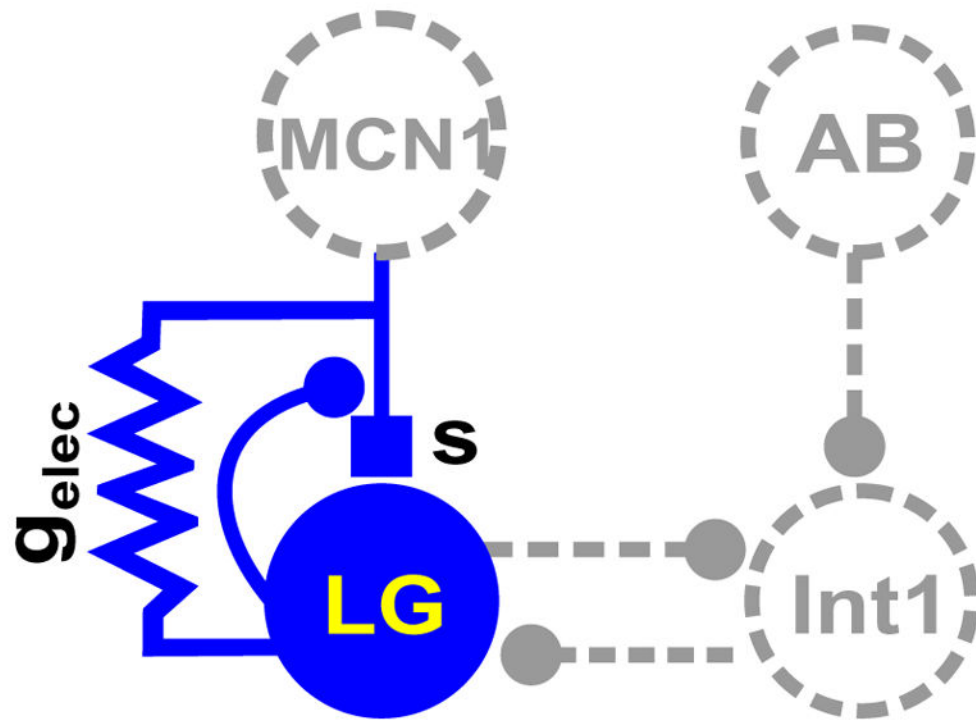


**Figure 1. Schematic diagram of the modeled network**

Solid elements are explicitly represented in the reduced two-dimensional model whereas dashed elements are defined as functions of the explicit variables. Filled small circles indicate synaptic inhibition, solid box is synaptic excitation and the resistor symbol indicates electrical gap junction coupling between the *MCN1* axon terminals and *LG*.

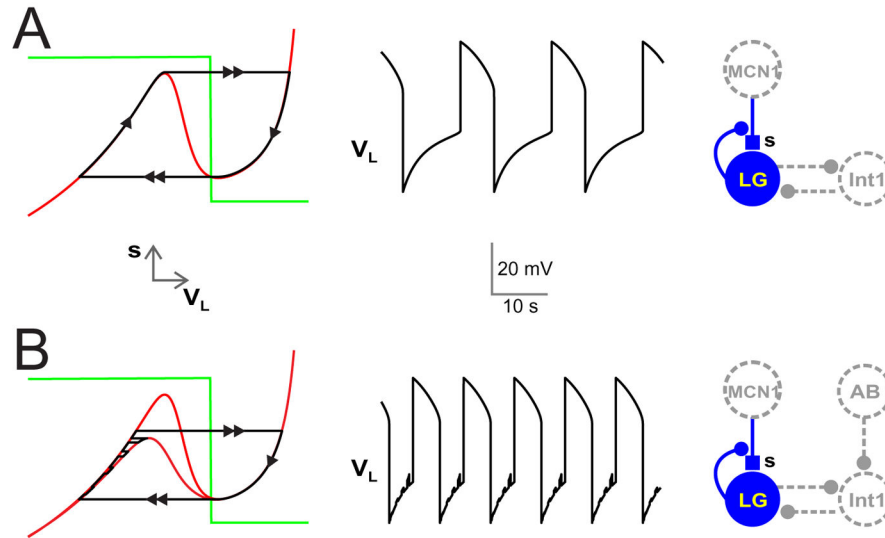


**Figure 2. Synaptic and electrical connectivity**

The synaptic and electrical connectivity of the gastric mill network along with nullclines and voltage trace of  $LG$  is shown. Schematic diagrams show that  $LG$  and  $INT1$  reciprocally inhibit one another.  $MCN1$  provides a slow modulatory excitation ( $s$ ) to  $LG$ . This excitation to  $LG$  is removed by presynaptic inhibition of this synapse by  $LG$ , when  $LG$  is active. (A) In the absence of rhythmic input from  $AB$  to  $INT1$ , the interaction between  $LG$ ,  $INT1$  and  $s$  produces oscillatory activity. The graph on the far left displays the  $V_L - s$  nullclines. The red curve shows the  $V_L$  nullcline whereas the green step curve shows the  $s$  nullcline. The solution trajectory is in black with the arrows indicating the direction of the trajectory and double arrows indicating the fast jumps. As the excitation  $s$  builds up, the solution trajectory slowly travels up the left branch of the  $V_L$  nullcline and jumps across to the right branch once the trajectory reaches the local maximum and  $LG$  transitions to its active phase ( $V_L > V_T$ ). Once  $LG$  is active, the excitatory input  $s$  slowly decays, causing the trajectory to slowly travel down the right branch of the  $V_L$  nullcline until it reaches the local minimum at which it jumps back to the left branch. The corresponding changes in  $V_L$  versus  $t$  is shown in the middle panel. (B) In the presence of the  $AB$  to  $INT1$  synaptic inhibition, during each pyloric cycle when  $AB$  inhibits  $INT1$ ,  $LG$  is released from  $INT1$  inhibition and the left branch of the  $V_L$  nullcline moves down (lower red  $V_L$  nullcline). The nullcline returns to its original uninhibited position (upper red  $V_L$  nullcline) once the  $AB$  inhibition turns off. In response, the solution trajectory slowly travels up the left branch of the  $V_L$  nullcline while making jumps in fast time between to upper and lower branch when the  $AB$  inhibition is on or off. As in panel A, the solution jumps across to the right branch once the trajectory reaches the local maximum. The trajectory then slowly travels down the right branch of the  $V_L$  nullcline until it reaches the local minimum at which it jumps back to the left branch. Note that the  $AB$  inhibition does not affect the right branch of the  $V_L$  nullcline (or the trajectory) because, when  $LG$  is active, it inhibits  $INT1$  thereby removing the functional effect of the  $AB$  to  $INT1$  synapse. The corresponding changes in  $V_L$  versus  $t$  is shown in the middle panel. Small depolarizations in the voltage of  $LG$  due to the  $AB$  input can be seen in the silent phase of its rhythm.

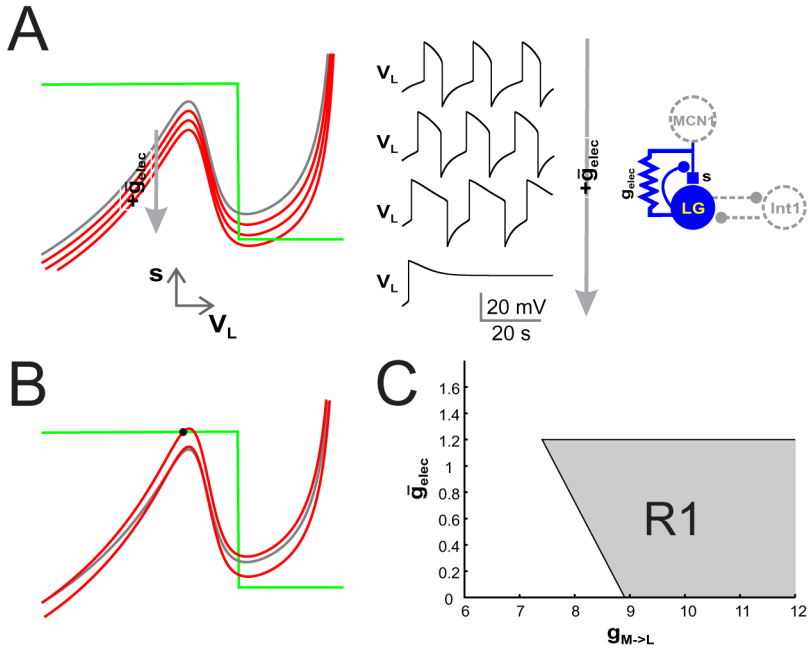


**Figure 3. The effect of non-voltage dependent electrical coupling**

Non-voltage dependent electrical coupling between *LG* and *MCN1* increases the *LG* burst duration and decreases the interburst duration. (A) The left panel shows the  $V_L - s$  nullclines for  $\bar{g}_{elec} = 0$  (grey curve; same as in Fig. 1A), 0.5, 1 and 1.5 (red curves). As the value of  $\bar{g}_{elec}$  increases, the  $V_L$  nullcline shifts down. Because the electrical coupling is non-voltage dependent, both the left and right branches of the  $V_L$  nullcline shift downward. The middle panel shows  $V_L$  vs  $t$  traces for the different values of  $\bar{g}_{elec}$ . As  $\bar{g}_{elec}$  increases the *LG* burst duration increases while its interburst duration decreases. (B) For  $\bar{g}_{elec} = 0$  and  $g_{M \rightarrow L}$  small (8.8 here, compared to 10 in panel A), a stable fixed point (filled circle) exists on the left branch of the  $V_L$  nullcline thereby preventing the existence of oscillations (upper nullcline). If the value of  $\bar{g}_{elec}$  is chosen to be large enough, the  $V_L$  nullcline is lowered and oscillations can occur. The  $V_L$  nullcline from Fig. 1A and panel A (with  $g_{M \rightarrow L} = 10$ ) is shown (in grey) for comparison. (C) The bifurcation diagram in  $g_{M \rightarrow L} - \bar{g}_{elec}$  space. The shaded region *R1* depicts the range of parameter values for which oscillations exist. The lower boundary along  $\bar{g}_{elec} = 0$  corresponds to the range of oscillations that exist when there is no electrical coupling. The left boundary corresponds to the set of saddle-node values along the local maximum of the  $V_L$  nullcline at  $s = 1$ . The top boundary corresponds to the set of saddle-node points when the minimum of the cubic nullcline is tangent to  $s = 0$ .



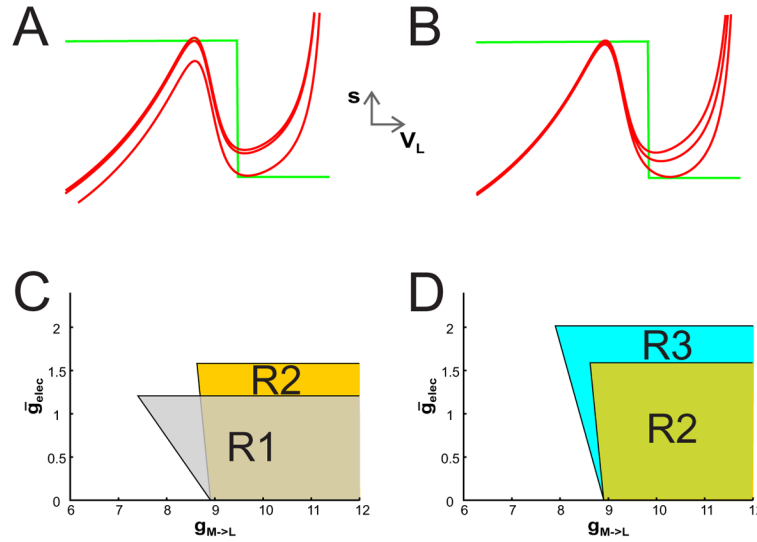


**Figure 4. The effect of voltage dependent electrical coupling between *LG* and the *MCN1* output to *LG***

(A) The  $V_L$  nullcline is shown for various values of  $\bar{g}_{elec}$  in the non-voltage dependent case (as in Fig. 2) with  $g_{M \rightarrow L} = 8.8$ . As the value of  $\bar{g}_{elec}$  increases, both the left and right branches of the  $V_L$  nullcline move down. The values of  $\bar{g}_{elec}$  shown are 0, 0.088 where oscillations first appear, and 1.2 where oscillations disappear due to the appearance of a stable fixed point on the right branch. (B) The  $V_L$  nullcline is shown for various values of  $\bar{g}_{elec}$  in the voltage dependent case. As the value of  $\bar{g}_{elec}$  increases, the right branch of the  $V_L$  nullcline shifts down much more than the left branch. As in panel A, the values of  $\bar{g}_{elec}$  shown are 0, 0.594 where oscillations first appear, and 1.57 where oscillations disappear due to the appearance of a stable fixed point on the right branch. (C) A bifurcation diagram in  $g_{M \rightarrow L} - \bar{g}_{elec}$  space is shown. The shaded region R1 depicts the range of parameter values for which oscillations exist for non-voltage dependent electrical coupling (same as in Fig. 3C) while the region R2 depicts the range for voltage dependent electrical coupling. The region R2 is more steeply sloped and the top boundary sits at a higher value of  $\bar{g}_{elec}$  than the region R1. (D) Region R3 depicts the range of parameter values for which oscillations exist when the  $n_{\infty}(V_L)$  curve is less steeply sloped. In this case, the left boundary of the oscillation region decreases to a value that is much closer to the voltage-independent case. The top boundary of R3 increases because larger values of  $\bar{g}_{elec}$  are required to generate oscillations.

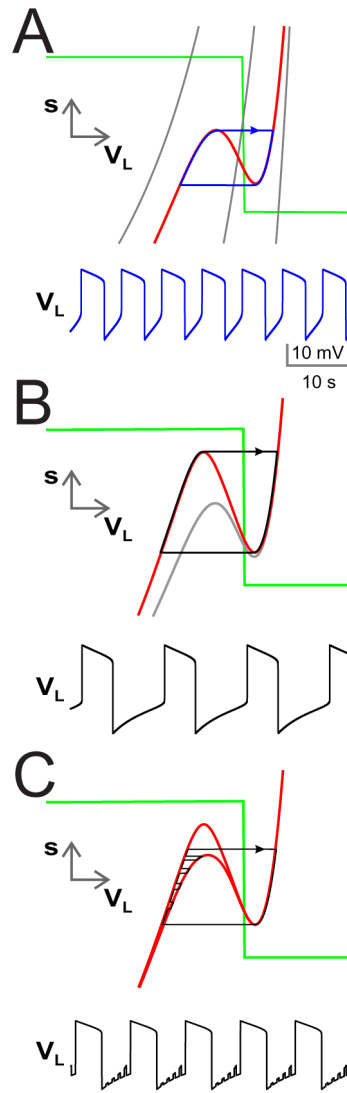


**Figure 5. Oscillations arising through the voltage-dependent coupling between MCN1 and LG when the INT1-LG HCO is ineffective**

(A) Input from *INT1* is removed by setting  $g_{I \rightarrow L} = 0$ . The  $V_L$  nullcline is shown for three values of  $\bar{g}_{elec}$  (weak, medium and strong) in the non-voltage dependent case (grey curves). In these cases, the  $V_L$  nullcline is monotonically increasing and oscillations cannot occur. When the electrical coupling is voltage dependent, the  $V_L$  nullcline is cubic even in the absence of reciprocal inhibition (red nullcline). Thus, oscillations can be generated through the electrical coupling together with the slow excitation ( $s$ ) from *MCN1*. (B) When the reciprocal inhibition is restored, the left branch of the  $V_L$  nullcline is raised (top red nullcline) thereby increasing both the *LG* burst and interburst durations. The trajectory must now reach the local maximum of the raised cubic in order to transition to the active state. The corresponding voltage trace is shown in the bottom panel. (C) In the presence of *AB* input to *INT1* in addition to the voltage dependent electrical coupling, the *LG* interburst duration is shortened because the solution trajectory is allowed to jump to the right branch at a time when the *LG* nullcline is lowered due to the *AB* inhibition of *INT1*.

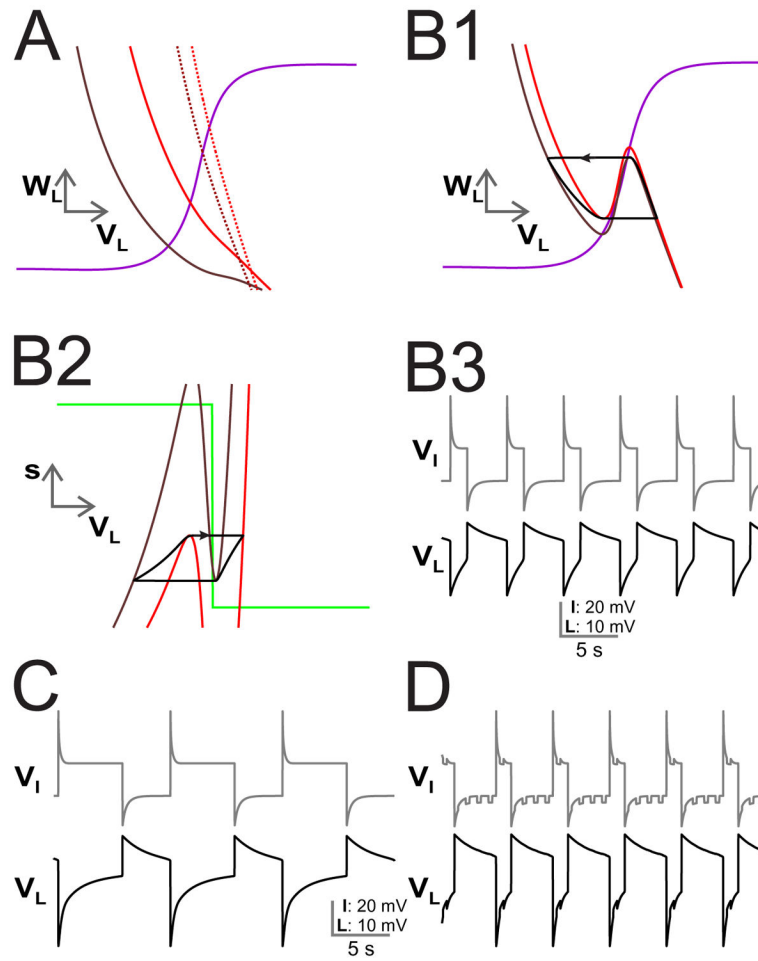


**Figure 6. Oscillations arising through the voltage-dependent coupling between *MCN1* and *LG* in the biophysical model**  
 (A) Input from *INT1* to *LG* is removed by setting  $g_{I \rightarrow L} = 0$ . For the non-voltage dependent case, the projection of  $V_L$  nullcline onto the  $V_L - W_L$  space is shown for different cases (solid brown  $\bar{g}_{elec} = 2.2, s = 0$ , solid red  $\bar{g}_{elec} = 2.2, s = 1$ , dashed brown  $\bar{g}_{elec} = 22, s = 0$ , dashed red  $\bar{g}_{elec} = 22, s = 1$ ). (B1) When the electrical coupling is voltage dependent, the  $V_L$  nullcline is cubic (brown larger  $s$ , red smaller  $s$ ). The trajectory transitions between branches from the local extrema points of the relevant  $V_L$  nullclines. (B2) The corresponding figure for the projection of the  $V_L$  nullcline onto the  $V_L - s$  space. (B3) Voltage traces for *INT1* and *LG* showing anti-phase oscillations. (C) The reciprocal inhibition from *INT1* to *LG* is restored, lengthening the *LG* interburst similar to Fig. 5B. (D) The presence of *AB* inhibition to *INT1*, shortens the *LG* interburst due to disinhibition as in Fig. 5C.

**Table 1**

Parameter values common to all simulations of the simple model

<i>intrinsic</i>	<i>inhibitory</i>	<i>excitatory</i>	<i>electrical</i>
$g_{rest,L} = 1$	$g_{L \rightarrow I} = 2$	$V_M = 10$	$g_{min} = 0.1$
$g_{rest,I} = 0.75$	$v_1 = -30$	$E_{exc} = 0$	$k_{el} = 5$
$E_{rest,L} = -60$	$k_1 = 8$	$V_T = -30$	volt. dep.
$E_{rest,I} = 10$	$v_2 = -25$	$\tau_r = 5,000$	$v_{el} = -30$
	$k_2 = 5$	$\tau_f = 3,500$	non-volt. dep.
	$v_3 = -35$		$v_{el} = -100$
	$k_3 = 3$		
	$E_{inh} = -80$		

Author Manuscript

Author Manuscript

Author Manuscript

Author Manuscript

**Table 2**

Parameter values common to all simulations of the Morris-Lecar model

<i>intrinsic</i>	<i>intrinsic</i>	<i>synaptic</i>	<i>electrical</i>
$g_{leak,L} = 3$	$I_{app,I} = 120$	$V_M = 10$	$g_{min} = 0.1$
$g_{leak,I} = 2$	$I_{app,L} = 100$	$E_{exc} = 20$	$k_{el} = 2$
$E_{leak} = -60$	$\varphi_I = 0.001$	$V_T = -10$	volt. dep.
$g_{Ca,I} = 4.4$	$\varphi_L = 0.0003$	$\tau_r = 5,000$	$v_{el} = -12$
$g_{Ca,L} = 0.5$	$wf_I = 10$	$\tau_r = 3,500$	non-volt. dep.
$E_{Ca} = 120$	$wf_L = -10$	$g_s = 5$	$v_{el} = -120$
$g_K = 8$		$g_{L \rightarrow I} = 1$	
$E_K = -84$		$\gamma = 5$	
$C = 20$		$v_{ith} = 25$	
$cv1 = -1.2$		$t_a = 10$	
$cv2 = 9$		$\alpha = 2$	
$cv3 = 3$		$\beta = 2$	
$cv4 = 11$		$E_{inh} = -80$	